

COORDINATED ASSEMBLY OF BRIGHTEST CLUSTER GALAXIES

MENG GU¹, CHARLIE CONROY¹ AND GABRIEL BRAMMER²

Accepted for publication in ApJL

ABSTRACT

Brightest Cluster Galaxies (BCGs) in massive dark matter halos are shaped by complex merging processes. We present a detailed stellar population analysis in the central region of Abell 3827 at $z \sim 0.1$, including five-nucleus galaxies involved in a BCG assembly. Based on deep spectroscopy from Multi Unit Spectroscopic Explorer (MUSE), we fit the optical spectra of 13 early-type galaxies (ETGs) in the central 70 kpc of the cluster. The stellar populations in the central $R = 1$ kpc of these ETGs are old (> 6 Gyr). Their $[\text{Fe}/\text{H}]$ increases with σ_* and stellar mass. More importantly, $[\alpha/\text{Fe}]$ of galaxies close to the cluster center do not seem to depend on σ_* or stellar mass, indicating that the cluster center shapes the $[\alpha/\text{Fe}]-\sigma_*$ and $[\alpha/\text{Fe}]-M_*$ relations differently than other environments where $[\alpha/\text{Fe}]$ is observed to increase with increasing σ_* or M_* . Our results reveal the coordinated assembly of BCGs: their building blocks are different from the general low mass populations by their high $[\alpha/\text{Fe}]$ and old ages. Massive galaxies thus grow by accreting preferentially high $[\alpha/\text{Fe}]$ and old stellar systems. The radial profiles also bear the imprint of the coordinated assembly. Their declining $[\text{Fe}/\text{H}]$ and flat $[\alpha/\text{Fe}]$ radial profiles confirm that the accreted systems have low metallicity and high $[\alpha/\text{Fe}]$ stellar contents.

Keywords: galaxies: clusters: individual (Abell 3827) — galaxies: stellar content — galaxies: evolution

1. INTRODUCTION

According to the Λ -Cold Dark Matter model, galaxy assembly is closely linked to the hierarchical growth of dark matter structures. Local massive early-type galaxies (ETGs) are considered to have evolved from the compact “red nuggets” at $z \approx 2$ by doubling their stellar masses and increasing their effective radii by a factor of 3–5 (e.g. van Dokkum et al. 2010; Patel et al. 2013). Recent simulations describe this transformation by the two-phase scenario (e.g. Naab et al. 2009; Oser et al. 2010, 2012), in which massive ETGs experience strong dissipational processes that lead to rapid and concentrated mass growth at high redshifts, and accrete low mass systems at later times to build up the outer envelopes. Brightest cluster galaxies (BCGs) are a special class of ETGs at the extreme high-mass end of the stellar mass function and in the densest environments. They have diffuse and extended envelopes (e.g. Schombert 1988) that can be explained by a series of merging events (e.g., Ostriker & Tremaine 1975; Hausman & Ostriker 1978; Dubinski 1998).

It is still ambiguous whether the low mass galaxies we observe today are intrinsically different from the building blocks of massive galaxies, or their surviving counterparts. One useful approach is to compare the abundance trends of their stellar contents, especially the ratio between α -elements to iron. $[\alpha/\text{Fe}]$ is used to indicate the star formation timescales due to its sensitivity to the time delay between SNe II and SNe Ia (e.g. Tinsley 1979). SNe II from massive stars yield both α -elements and Fe, while SNe Ia from low mass binary systems contribute mostly Fe on longer timescales. High $[\alpha/\text{Fe}]$ in old stellar population suggests short star formation timescales in the past. Stellar population analysis has revealed correlations between stellar population properties and stellar mass or stellar velocity dispersion (e.g. Trager et al. 2000; Worthey & Colobert 2003; Thomas et al. 2005; Schiavon 2007; Thomas

et al. 2010; Conroy et al. 2014; McDermid et al. 2015) in a way that massive galaxies are older, more metal rich and more α -enhanced compared to low mass galaxies. If these trends are universal for all environments and epochs, an apparent tension under the hierarchical assembly paradigm would emerge: the building blocks of massive galaxies, especially the BCGs would have “diluted” the $[\alpha/\text{Fe}]$ at the high mass end, and/or would produce steep $[\alpha/\text{Fe}]$ gradients. This would make it difficult to reconcile with the general observational facts that more massive galaxies are more α -enhanced.

The Milky Way satellite dwarf galaxies were once thought to be the surviving counterparts of Galactic building blocks until studies revealed their stellar populations occupy different locations from Milky Way halo stars on the $[\alpha/\text{Fe}]$ vs. $[\text{Fe}/\text{H}]$ diagram (e.g. Tolstoy et al. 2009). Looking beyond the Milky Way, Liu et al. (2016) showed that the $[\alpha/\text{Fe}]$ of low mass ETGs in the Virgo cluster depend on the distance to the cluster center and the $[\alpha/\text{Fe}]-\sigma_*$ relation in this cluster has larger scatter, indicating that the densest environments quench low mass galaxies earlier than other environments. From these studies it seems that the assembly of massive galaxies are coordinated in a way that their building blocks have early truncated star formation histories, making them a particular sample with high $[\alpha/\text{Fe}]$ among the low mass systems.

In this Letter, we present stellar population analysis on 13 ETGs in Abell 3827. Five of them are involved in a rarely observed BCG assembly from multiple mergers, therefore we are fortunate to directly analyze the building blocks of a prospective BCG. $[\text{Mg}/\text{Fe}]$ is used as a tracer of $[\alpha/\text{Fe}]$. We compare the stellar population scaling relations in this special environment to the general samples in previous work. We assume a flat Λ CDM cosmology with $h = 0.73$, $\Omega_m = 0.27$, $\Omega_\Lambda = 0.73$. The redshift of Abell 3827 is $cz = 29500$ km s⁻¹ (Struble & Rood 1999). The distance is assumed to be 433 Mpc. This corresponds to a distance modulus of 38.18 mag and a scale of 1.74 kpc arcsec⁻¹. All magnitudes in this paper are in the AB system. The mass center of Abell 3827 is assumed to be at RA = 22^h01^m52.90^s, DEC = -59^d56^m44.89^s (Massey et al.

¹ Department of Astronomy, Harvard University, Cambridge, MA 02138, USA

² Space Telescope Science Institute, 3700 San Martin Drive, Baltimore, MD 21218, USA

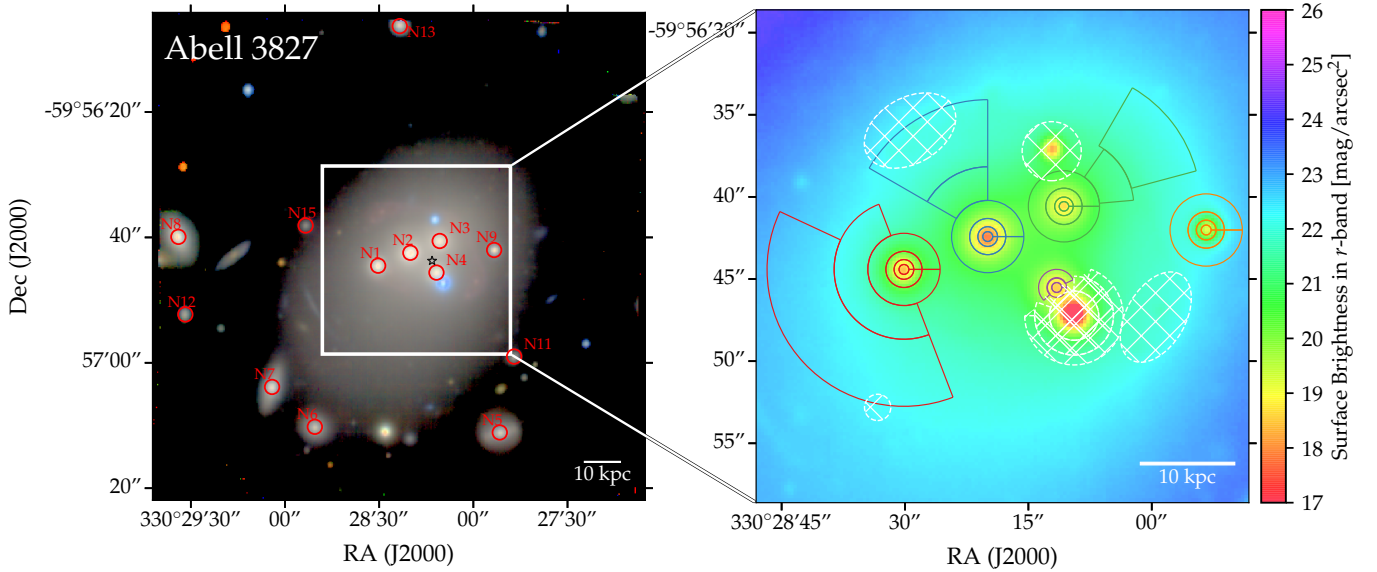


Figure 1. Left panel: Overview of the locations of ETGs studied in this paper on a SDSS-*riz* composite image derived from the MUSE datacube. Red circles enclose $R = 2$ kpc. Right panel: Zoomed-in SDSS-*r* band surface brightness map derived from the MUSE datacube. Solid lines enclose stacked regions for radial profiles. White hatched regions highlight masked out spaxels.

2015). We assume the *r* band solar absolute magnitude to be 4.76 mag (Blanton et al. 2003).

2. DATA AND METHODS

We use the datacube obtained by the Multi-Unit Spectroscopic Explorer (MUSE) Integral Field Unit (IFU) spectrograph (Bacon et al. 2010; Le Fèvre et al. 2013) on the European Southern Observatory (ESO) Very Large Telescope (VLT). Abell 3827 was observed in 2015 (ESO programme 295.A-5018(A), PI: Richard Massey, Massey et al. (2015, 2017)), centered at RA = $22^h03^m14.65^s$, DEC = $-59^d56^m43.19^s$. We reduce and combine the data using MUSE Pipeline *muse-2.2* (Weilbacher et al. 2014, 2016). According to Massey et al. (2017), observations were taken in dark time with seeing around $0.7''$. The total integration time in the final datacube is 3.2 hr. The field of view (FoV) is $1' \times 1'$. The wavelength coverage is 475–935 nm, sampled at $1.25\text{\AA}/\text{pixel}$, with mean spectral resolution ~ 3000 at the optical wavelength range. The spatial pixel size is $0.2'' \times 0.2''$. Due to the small FoV we limit the sky regions during the data reduction, by setting *skymodel_fraction* to 0.01. As a result, the surface brightness profiles in of the MUSE datacube are consistent with the *HST/ACS* image³ out to $\mu_{F606W} = 24\text{mag arcsec}^{-2}$, with $\Delta\mu_{F606W} \approx 0.22\text{mag arcsec}^{-2}$ at $\mu_{F606W} = 24\text{mag arcsec}^{-2}$.

Galaxies in Abell 3827 and foreground stars are identified using SExtractor (Bertin & Arnouts 1996). 13 ETGs in Abell 3827 are selected for further analysis. They are all confirmed spectroscopically and are shown in Figure 1. We mask out foreground stars and background lensed galaxies (whited hatched region). To study the radial profiles of stellar populations, we analyze the spectra by binning spaxels in radial directions for N1–N4 and N9. The binning scheme is shown in the right panel of Figure 1.

³ Based on observations made with the NASA/ESA Hubble Space Telescope, obtained from the Mikulski Archive at the Space Telescope Science Institute, which is operated by the Association of Universities for Research in Astronomy, Inc., under NASA contract NAS 5–26555. These observations are associated with program 12817.

To model galaxies spectra we use the absorption line fitter (*alf*, Conroy & van Dokkum 2012; Conroy et al. 2014, 2018). *alf* enables stellar population modeling of the full spectrum for stellar ages $> 1\text{Gyr}$ and for metallicities from ~ -2.0 to $+0.25$. Parameter space is explored using a Markov Chain Monte Carlo algorithm (*emcee*, Foreman-Mackey et al. 2013). *alf* adopts the MIST stellar isochrones (Choi et al. 2016) and uses a new spectral library (Villaume et al. 2017) that includes continuous wavelength coverage from $0.35 - 2.4\mu\text{m}$ over a wide range in metallicity, which taken from new IRTF NIR spectra for stars in the MILES optical spectral library (Sánchez-Blázquez et al. 2006). Theoretical elemental response functions were computed with the ATLAS and SYNTHE programs (Kurucz 1970, 1993). They tabulate the effect on the spectrum of enhancing each of the individual elements. With *alf* in “full” mode we fit for parameters including a two burst star formation history, the redshift, velocity dispersion, overall metallicity, 18 individual element abundances, several IMF parameters (Conroy et al. 2018). Throughout this paper, we use *alf* with the IMF fixed to the Kroupa (2001) form. We use flat priors within these ranges: $-10^3 - 10^5$ km/s for recession velocity, 100–1000 km/s for velocity dispersion, 1.0–14 Gyr for age and $-1.8 - +0.3$ for metallicities. For each spectrum we fit a continuum in the form of a polynomial to the ratio between model and data. The order of polynomial is $(\lambda_{max} - \lambda_{min})/100\text{\AA}$. During each likelihood call the polynomial divided input spectrum and model are matched. The continuum normalization occurs in three separate wavelength intervals, 4300–5080Å, 5080–5700Å and 5700–6700Å.

Five galaxies have central velocity dispersion smaller than the resolution of the models (100 km/s): N5, N6, N11, N12, and N15. Their spectra are smoothed by convolving a wavelength dependent Gaussian kernel with $\sigma = \sqrt{100^2 - \sigma_i^2}$ prior to the modeling, where σ_i is the wavelength dependent instrumental resolution.

To study the spatial distribution of stellar population parameters, spectra in adjacent spaxels are binned by Voronoi tessellation (Cappellari & Copin 2003). The mean S/N in ob-

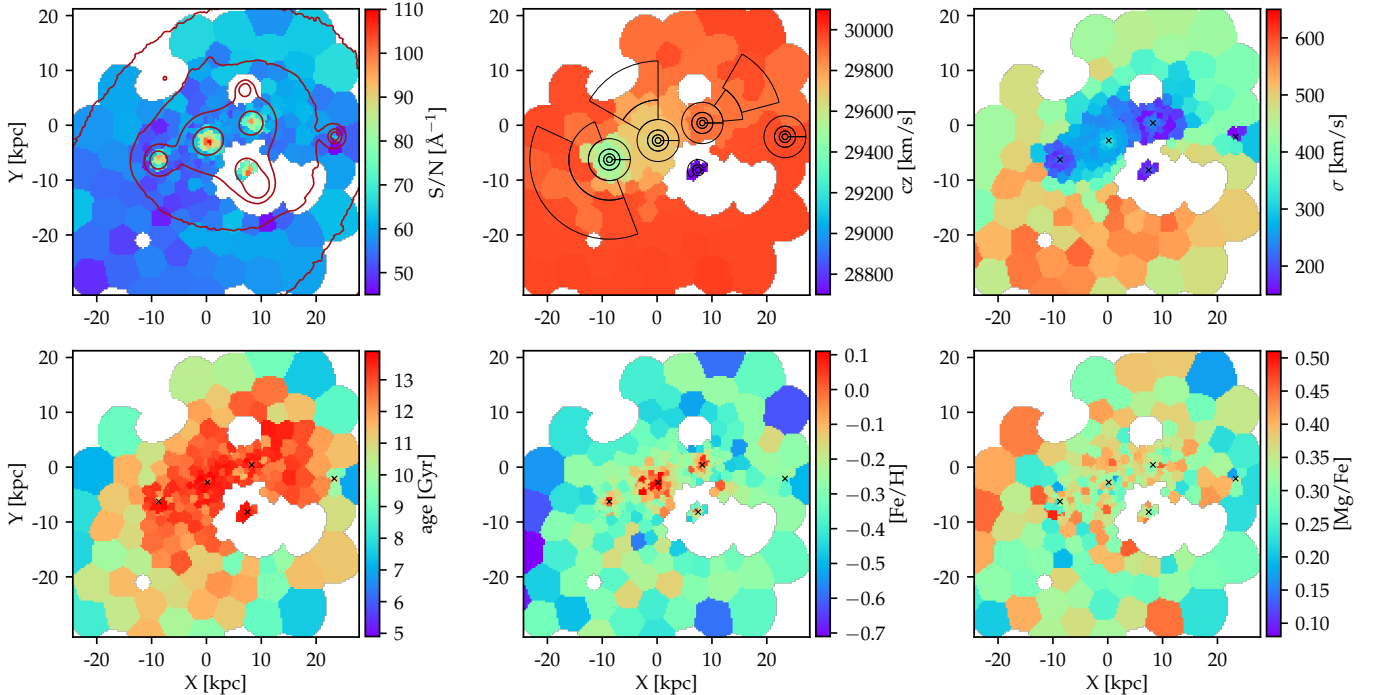


Figure 2. From top left to bottom right: Spatial distribution of the mean S/N per bin in observed frame 4500–5000 Å, recession velocity cz , velocity dispersions σ_* , stellar ages, [Fe/H] and [Mg/Fe]. Contours (top left) indicate the surface brightness levels of $\mu_r = 20, 21, 22$ and 23 mag arcsec $^{-2}$. Black lines (top middle) enclose stacked regions for the radial profiles. Centers of five nuclei galaxies are cross-marked. The typical errors of $\log(\text{age}/\text{Gyr})$, [Fe/H] and [Mg/Fe] are ≈ 0.03 dex in bins with $S/N > 100 \text{Å}^{-1}$. In regions where σ_* is large, the errors are ≈ 0.15 dex in bins with $S/N \sim 50 \text{Å}^{-1}$.

served frame 4500–5000Å of this binning scheme is shown in the top left panel of Figure 2. The S/N is between 40Å^{-1} and 110Å^{-1} . In addition to foreground stars and lensed galaxies, we also exclude bins where foreground and background galaxies overlap with each other, e.g., some spaxels between N4 and N2. Only bins where the best-fit spectra and residuals are visually consistent with data and data uncertainties are shown here. The low S/N at the outskirts ($R > 3$ kpc) of low mass ETGs makes it hard to derive reliable mass to light ratio (M/L). Therefore, we assume constant M/L as a function of radius and adopt the M/L measured within $R = 1$ kpc. The stellar masses within $R = 5$ kpc of the 13 ETGs are derived by multiplying the rest-frame r band total integrated luminosity within $R = 5$ kpc, by the best-fit M/L in r band within $R = 1$ kpc.

3. RESULTS AND DISCUSSION

We present results in this section. Objects N1, N2, N3, N4 and N9 have the closest projected distances to the mass center (≤ 18 kpc). Their recession velocities relative to the cluster center ($cz = 29500$ km/s) are $cz = -45^{+4}_-3$ km/s, 167^{+3}_-3 km/s, 359^{+3}_-3 km/s, -830^{+4}_-4 km/s and 452^{+4}_-4 km/s, respectively. Given their small projected distances to the cluster center and very similar velocities, they are on their way to form a massive BCG in the near future. If we estimate the time it would take based the dynamical friction time (Binney & Tremaine 1987), the 5 ETGs will merge within 1 Gyr. Therefore we assume N1–N4 and N9 are building blocks of a prospective BCG with $\log(M_*/M_\odot) \approx 11.7$.

Spatial distribution of the following parameters are shown in Figure 2: cz , σ_* , stellar age, [Fe/H] and [Mg/Fe], focusing on $D \approx \pm 25$ kpc around the cluster center. The cz distribution shows that the five ETGs are all members of the cluster.

The σ_* map shows that σ_* declines outwards from the center of N1–N4 within $R \sim 2$ kpc, and rise towards the outskirts, reaching to ~ 400 – 500 km/s. This shows that the stars in the outskirts are tracing the gravitational potential of the cluster, instead of any individual galaxy, and describes the formation of the cD envelope, or the intracluster light component that have been measured in other galaxy clusters (e.g. Kelson et al. 2002). Due to the large σ_* , the typical errors of $\log(\text{age}/\text{Gyr})$, [Fe/H] and [Mg/Fe] are ~ 0.1 dex in bins with $S/N \approx 50 \text{Å}^{-1}$. The stellar age distribution shows this region is uniformly old. From the [Fe/H] distribution we see declining [Fe/H] from the galaxy centers outwards, indicating that the inner regions of the galaxies are more metal rich than the cD envelop where the stellar content is likely from disrupted low mass systems. The distribution of [Mg/Fe] shows that the α -abundance in this region are generally high, with no particular pattern of differences between the galaxy centers and the cD envelope, indicating that the stellar content have short star formation timescales in general.

Figure 3 shows the main result. We compare the median stellar population parameters within $R = 1$ kpc, including [Fe/H], stellar ages and [Mg/Fe] as a function of galaxy velocity dispersion σ_* and galaxy stellar mass. Colors indicate the projected distance to the cluster mass center. Previous studies found scaling relations between stellar population properties and the central σ_* : the stellar components in galaxies with higher central σ_* are older, more metal rich and more α -enhanced (e.g. Trager et al. 2000; Thomas et al. 2005; Schiavon 2007; Graves et al. 2009; Conroy et al. 2014). We compare our results to previous studies in Figure 3, including a large sample of morphologically selected SDSS ETGs in Thomas et al. (2005) (red dash-dotted line), ETGs in ATLAS 3D by McDermid et al. (2015) (blue circles), 12

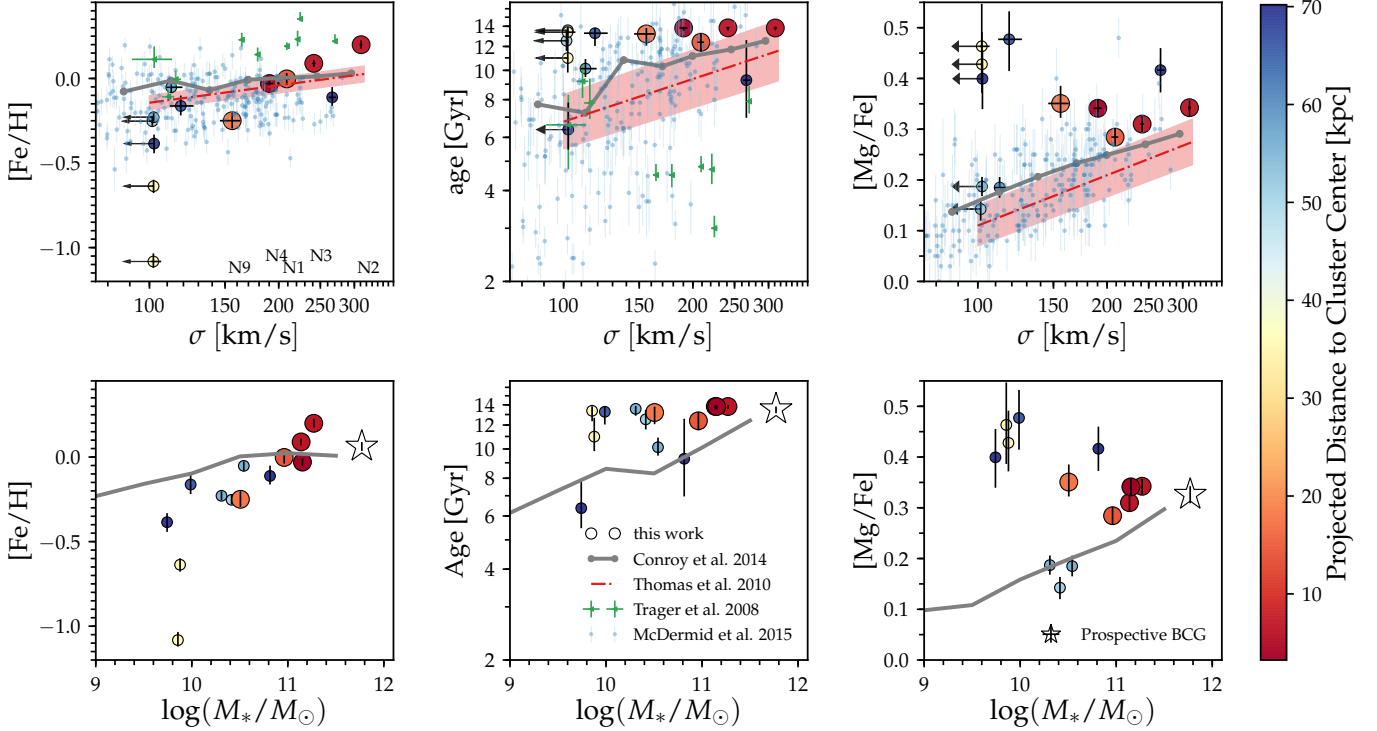


Figure 3. Top: Relationships between σ_* and stellar population parameters: [Fe/H], stellar ages and [Mg/Fe]. Bottom: Relationships between stellar mass measured within $R = 5$ kpc and stellar population parameters measured within $R = 1$ kpc. Colors indicate the projected distance from the center of galaxies to the mass center of the cluster. 13 ETGs in our sample are compared to a large sample of morphologically selected SDSS ETGs in [Thomas et al. \(2005\)](#) (red dash-dotted line), ETGs in ATLAS^{3D} by [McDermid et al. \(2015\)](#) (blue circles), 12 ETGs in the Coma cluster by [Trager et al. \(2008\)](#) (green triangles) and updated results from stacked SDSS ETGs that are binned in σ_* and stellar mass ([Conroy et al. 2014](#)).

ETGs in the Coma cluster by [Trager et al. \(2008\)](#) (green triangles). We estimate [Fe/H] in the above literatures using Eq 4 in [Thomas et al. \(2002\)](#) assuming the factor $A = 0.94$ ([Trager et al. 2000](#)). We also compare to stacked SDSS ETGs that are binned in σ_* and stellar mass in [Conroy et al. \(2014\)](#), except that they are fit with the up-to-date `alf` with upgraded response functions.

For stellar age and [Fe/H], our results agree with the trends found in the general ETG populations: galaxies with higher central stellar velocity dispersion or larger stellar mass are older and more metal rich. For [Mg/Fe] our results are distinctly different from ETGs in the field. The [Mg/Fe] of galaxies within ~ 40 kpc to the cluster center have high [Mg/Fe], even indicating a trend that smaller galaxies are more [Mg/Fe] enhanced. If we assume the variation of [Mg/Fe] is due to the differences of star formation timescale (e.g. [Thomas et al. 2005](#)), Figure 3 illustrates that compared to galaxies in all environment, the ETGs with lower σ_* or stellar masses within ~ 40 kpc in Abell 3827 are quenched as early (if not more) as more massive galaxies. Our results highlight the effect of “environmental quenching” (e.g. [Peng et al. 2010](#)) on low mass galaxies, possibly due to the complex interplay between processes such as ram pressure stripping and strangulation. The high $[\alpha/\text{Fe}]$ and old stellar ages make the building blocks very different from low mass galaxies in general, and are possibly due to early quenching by the dense environment.

As described earlier N1–N4 and N9 are very likely building blocks of a BCG in the future. Although multiple nucleus are rarely observed, it has been predicted by recent simulations that major merger plays an important role on buildup of massive galaxies (e.g. [Rodríguez-Gomez et al. 2016](#)). We

estimate the stellar population properties of the prospective BCG through weighting the properties of the five ETGs by luminosity. The lower limit of its stellar mass is estimated using the total stellar mass of N1–N4 and N9 within $R = 5$ kpc: $\log(M_*/M_\odot) \approx 11.7$. The diffuse component is not included due to the contamination from the lensed galaxies and the foreground stars. The predictions are shown as black stars in Figure 3. This prospective BCG would fall on all the empirical trends between stellar population parameters and stellar mass.

The coordinated assembly picture can be described by the schematic diagrams in Figure 5: the building blocks of BCGs are low mass galaxies in a special environment—cluster centers. They follow a relatively flat relation between $[\alpha/\text{Fe}]$ or stellar age and stellar mass (red box), which are distinct from the relations followed by galaxies in the fields (blue box). The right panel shows the expected radial profiles of the massive ETGs: As the low mass systems in the cluster center accrete onto the outskirts of massive ETGs, the coordinated assembly produces flat radial profiles of stellar age and $[\alpha/\text{Fe}]$ (red), whereas if the accreted systems are random draws from the low mass galaxy sample in all environments the profiles of stellar age and $[\alpha/\text{Fe}]$ would decline with radius.

The radial profiles of stellar population properties confirm the coordinated assembly picture. Figure 4 shows the radial profiles of velocity dispersion σ_* , stellar ages, [Fe/H], and [Mg/Fe] for N1–N4 and N9. The binning schemes are shown in the right panel of Figure 1. These profiles are compared to that of 6 ETGs in [van Dokkum et al. \(2017b\)](#). Note that we only show the combined profiles from both sides of the 6 ETGs. Due to the contamination of the foreground stars

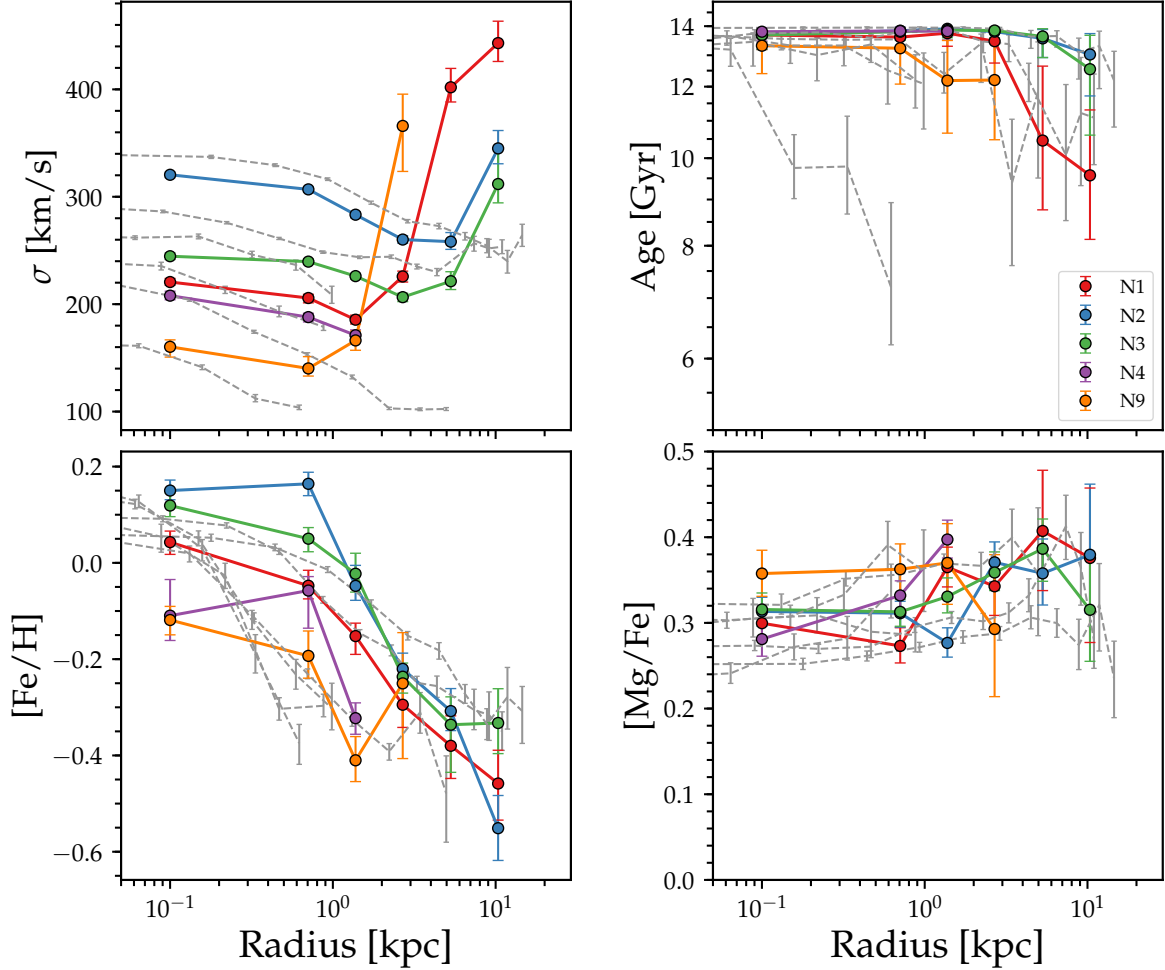


Figure 4. Radial profiles of stellar population parameters. From top left to bottom right: stellar velocity dispersions σ_* , stellar ages, $[\text{Fe}/\text{H}]$ and $[\text{Mg}/\text{Fe}]$ as functions of distance to the center of five galaxies that are closest to the cluster center. Gray dashed lines represent the radial profiles of six ETGs in van Dokkum et al. (2017a).

and background lensed galaxies, we are not able to extend the radial trends beyond 14 kpc. However, we can already see rising velocity dispersion profiles built up for N1–N3, which is consistent with the expected cD galaxy profiles (e.g. Kelson et al. 2002). The stellar ages profiles indicate that the ages of the 5 ETGs are generally old from the center to the outskirts. $[\text{Fe}/\text{H}]$ declines with the radius, and seems to depend on the

central velocity dispersions within $R = 2$ kpc. This is consistent with the two phase formation scenario (e.g. Naab et al. 2009; van der Wel et al. 2014) that the inner regions are mostly build up by the dissipational process at high redshifts, thus strongly depend on the central stellar velocity dispersions, and the outskirts are dominated by accretion of small stellar systems. $[\text{Mg}/\text{Fe}]$ profiles are generally flat. Flat $[\alpha/\text{Fe}]$ profiles have also been observed previously (e.g. Sánchez-Blázquez et al. 2007; Greene et al. 2015). This is consistent with the coordinated assembly picture.

4. SUMMARY

We have presented detailed stellar population studies for 13 ETGs in Abell 3827 using the optical spectra from MUSE on the VLT. The sample includes five ETGs that are involved in an ongoing assembly of a BCG. Our conclusions are summarized as follows:

- The 13 ETGs are spectroscopically confirmed members of Abell 3827. Their stellar age and $[\text{Fe}/\text{H}]$ fall on empirical trends that galaxies with higher σ_* or stellar mass are older and more metal rich. However, ETGs within 40 kpc from the cluster center show higher $[\text{Mg}/\text{Fe}]$ compared to the $[\text{Mg}/\text{Fe}]$ – σ_* and $[\text{Mg}/\text{Fe}]$ – M_* relations in the field.

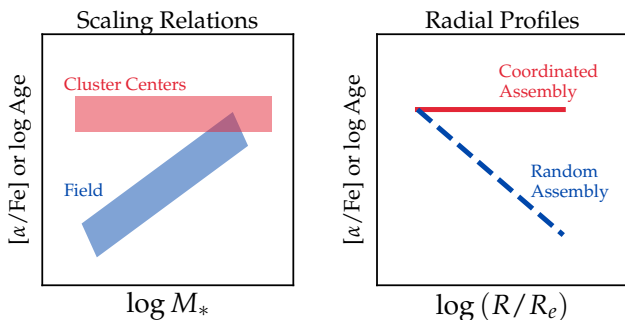


Figure 5. Schematic diagrams for scaling relations of $[\alpha/\text{Fe}]$ or $\log(\text{age})$ versus stellar mass in different environments (left), and the radial profile of $[\alpha/\text{Fe}]$ or $\log(\text{age})$ a massive ETG would build up (right) if it accreted systems randomly in all environments (blue), or coordinately from a sample of low mass galaxies that are quenched early on by the dense environments (red).

- From the spatial distribution in the central region of the cluster, the stellar populations in the diffuse stellar light of Abell 3827 are generally old and α -enhanced.
- We show the radial profiles of σ_* , stellar age, [Fe/H] and [Mg/Fe] that are consistent with previous studies. The flat stellar age and [Mg/Fe] profiles confirm the coordinated assembly picture.
- Our results highlight the effect of “environmental quenching”, and reveal the coordinated assembly of BCGs: the building blocks of the prospective BCG in Abell 3827 are distinct from the general low mass systems by high $[\alpha/\text{Fe}]$ due to early quenching by the dense environment.

Future spectroscopic observations of cluster centers will place constraints on the formation history of massive galaxies, and will shed additional light on the general picture of coordinated assembly.

M.G. acknowledges support from the National Science Foundation Graduate Research Fellowship. C.C. acknowledges support from NASA grant NNX15AK14G, NSF grant AST-1313280, and the Packard Foundation.

This research has made use of the services of the ESO Science Archive Facility, based on observations collected at the European Organization for Astronomical Research in the Southern Hemisphere under ESO programme 295.A-5018(A), PI: Richard Massey, and based on data obtained from the ESO Science Archive Facility under request number 345883. The computations in this paper were run on the Odyssey cluster supported by the FAS Division of Science, Research Computing Group at Harvard University.

REFERENCES

- Bacon, R., Accardo, M., Adjali, L., et al. 2010, in *SPIE Astronomical Telescopes + Instrumentation*, ed. I. S. McLean, S. K. Ramsay, & H. Takami (SPIE), 773508
- Bertin, E., & Arnouts, S. 1996, *Astronomy and Astrophysics Supplement Series*, 117, 393
- Binney, J., & Tremaine, S. 1987, Princeton, NJ, Princeton University Press, 1987, 747 p.
- Blanton, M. R., Hogg, D. W., Bahcall, N. A., et al. 2003, *The Astrophysical Journal Letters*, 592, 819
- Cappellari, M., & Copin, Y. 2003, *Monthly Notices of the Royal Astronomical Society*, 342, 345
- Choi, J., Dotter, A., Conroy, C., et al. 2016, *ApJ*, 823, 102
- Conroy, C., Graves, G. J., & van Dokkum, P. G. 2014, *The Astrophysical Journal Letters*, 780, 33
- Conroy, C., & van Dokkum, P. 2012, *The Astrophysical Journal Letters*, 747, 69
- Conroy, C., Villaume, A., van Dokkum, P. G., & Lind, K. 2018, *ApJ*, 854, 139
- Dubinski, J. 1998, *The Astrophysical Journal Letters*, 502, 141
- Foreman-Mackey, D., Hogg, D. W., Lang, D., & Goodman, J. 2013, *Publications of the Astronomical Society of the Pacific*, 125, 306
- Graves, G. J., Faber, S. M., & Schiavon, R. P. 2009, *The Astrophysical Journal Letters*, 693, 486
- Greene, J. E., Janish, R., Ma, C.-P., et al. 2015, *The Astrophysical Journal Letters*, 807, 11
- Hausman, M. A., & Ostriker, J. P. 1978, *The Astrophysical Journal Letters*, 224, 320
- Kelson, D. D., Zabludoff, A. I., Williams, K. A., et al. 2002, *The Astrophysical Journal Letters*, 576, 720
- Kroupa, P. 2001, *Monthly Notices of the Royal Astronomical Society*, 322, 231
- Kurucz, R. L. 1970, *SAO Special Report*, 309
- . 1993, Kurucz CD-ROM, Cambridge, MA: Smithsonian Astrophysical Observatory, lc1993, December 4, 1993
- Le Fèvre, O., Cassata, P., Cucciati, O., et al. 2013, *Astronomy & Astrophysics*, 559, A14
- Liu, Y., Peng, E. W., Blakeslee, J., et al. 2016, *The Astrophysical Journal Letters*, 818, 179
- Massey, R., Williams, L., Smit, R., et al. 2015, *Monthly Notices of the Royal Astronomical Society*, 449, 3393
- Massey, R., Harvey, D., Liesenborgs, J., et al. 2017, 1708.04245
- McDermid, R. M., Alatalo, K., Blitz, L., et al. 2015, *Monthly Notices of the Royal Astronomical Society*, 448, 3484
- Naab, T., Johansson, P. H., & Ostriker, J. P. 2009, *ApJ*, 699, L178
- Oser, L., Naab, T., Ostriker, J. P., & Johansson, P. H. 2012, *ApJ*, 744, 63
- Oser, L., Ostriker, J. P., Naab, T., Johansson, P. H., & Burkert, A. 2010, *ApJ*, 725, 2312
- Ostriker, J. P., & Tremaine, S. D. 1975, *The Astrophysical Journal Letters*, 202, L113
- Patel, S. G., van Dokkum, P. G., Franx, M., et al. 2013, *ApJ*, 766, 15
- Peng, Y.-j., Lilly, S. J., Kovac, K., et al. 2010, *The Astrophysical Journal Letters*, 721, 193
- Rodriguez-Gomez, V., Pillepich, A., Sales, L. V., et al. 2016, *Monthly Notices of the Royal Astronomical Society*, 458, 2371
- Sánchez-Blázquez, P., Forbes, D. A., Strader, J., Brodie, J., & Proctor, R. 2007, 377, 759
- Sánchez-Blázquez, P., Peletier, R. F., Jiménez-Vicente, J., et al. 2006, *Monthly Notices of the Royal Astronomical Society*, 371, 703
- Schiavon, R. P. 2007, *ApJS*, 171, 146
- Schombert, J. M. 1988, *ApJ*, 328, 475
- Struble, M. F., & Rood, H. J. 1999, *ASTROPHYS J SUPPL S*, 125, 35
- Thomas, D., Maraston, C., & Bender, R. 2002, arXiv, 897
- Thomas, D., Maraston, C., Bender, R., & Mendes de Oliveira, C. 2005, 621, 673
- Thomas, D., Maraston, C., Schawinski, K., Sarzi, M., & Silk, J. 2010, *Monthly Notices of the Royal Astronomical Society*
- Tinsley, B. M. 1979, *ApJ*, 229, 1046
- Tolstoy, E., Hill, V., & Tosi, M. 2009, *Annu. Rev. Astro. Astrophys.*, 47, 371
- Trager, S. C., Faber, S. M., & Dressler, A. 2008, *Monthly Notices of the Royal Astronomical Society*, 386, 715
- Trager, S. C., Faber, S. M., Worthey, G., & González, J. J. 2000, *The Astronomical Journal*, 119, 1645
- van der Wel, A., Franx, M., van Dokkum, P. G., et al. 2014, *ApJ*, 788, 28
- van Dokkum, P., Conroy, C., Villaume, A., Brodie, J., & Romanowsky, A. J. 2017a, *ApJ*, 841, 68
- van Dokkum, P., Abraham, R., Romanowsky, A. J., et al. 2017b, *ApJ*, 844, L11
- van Dokkum, P. G., Whitaker, K. E., Brammer, G., et al. 2010, *ApJ*, 709, 1018
- Villaume, A., Conroy, C., Johnson, B., et al. 2017, *ASTROPHYS J SUPPL S*, 230, 23
- Weilbacher, P. M., Streicher, O., & Palsa, R. 2016, *Astrophysics Source Code Library*
- Weilbacher, P. M., Streicher, O., Urrutia, T., et al. 2014, *From Stardust to Planetesimals*, 485, 451
- Worthey, G., & Collobert, M. 2003, *ApJ*, 586, 17